Electronic Supplementary Information

rGO Coated Cotton Fabric and Thermoelectric Module Arrays for Efficient Solar Desalination and Electricity Generation

Ahmed Mortuza Saleque[1,2a,b], Amrit Kumar Thakur[3], R. Saidur[4a,b], Mohammad Ismail Hossain[1,5], Wayesh Qarony[6], Md Shamim Ahamed[7], Iseult Lynch[8a,b], Y. Ma[3], Yuen Hong Tsang[2a,b,*]

1.) Department of Electrical and Computer Engineering, University of California, Davis, CA 95616, USA

2a.) Department of Applied Physics, Photonic Research Institute, and Materials Research Center, The Hong Kong Polytechnic University, Hung Hom, Kowloon, Hong Kong

2b.) Shenzhen Research Institute, The Hong Kong Polytechnic University, 518057 Shenzhen, Guangdong, People's Republic of China

3.) Department of Mechanical Engineering, University of California, Merced, CA, 95343, USA

4a.) Research Center for Nano-Materials and Energy Technology (RCNMET), School of Engineering and Technology, Sunway University, Bandar Sunway, Petaling Jaya 47500, Selangor Darul Ehan, Malaysia

4b.) School of Engineering, Lancaster University, Lancaster LA1 4YW, UK

5.) Research & Development, Meta Materials Inc., Pleasanton, CA 94588, USA

6.) Department of Electrical Engineering and Computer Sciences, University of California, Berkeley, CA 94720, USA

7.) Department of Biological and Agricultural Engineering, University of California, Davis, CA 95616, USA

8a.) School of Geography, Earth and Environmental Sciences, University of Birmingham, Edgbaston, B15 2TT Birmingham, UK

8b.) Institute for Global Innovation, University of Birmingham, Edgbaston, B15 2TT Birmingham, UK

*.) Corresponding author.

E-mail address: yuen.tsang@polyu.edu.hk (Y. H. Tsang).

Note S1. UV-Vis absorption spectrum of graphene oxide (GO) and reduced graphene oxide (rGO)

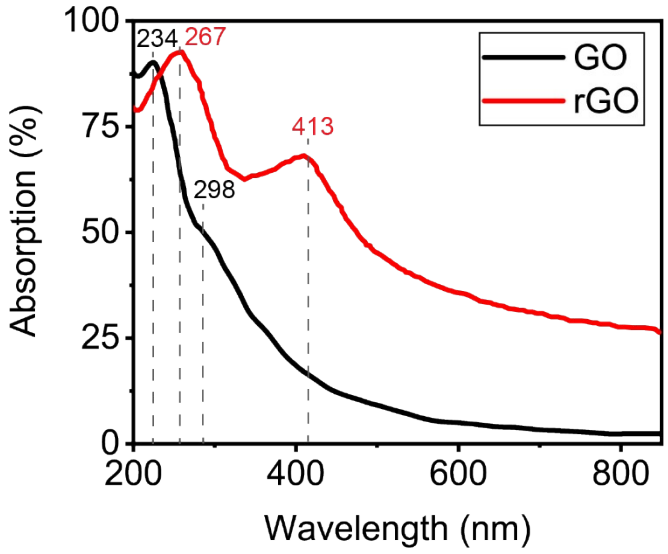

Figure S1. UV-Vis absorption spectrum of GO and rGO.

Note S2. Evaporation performance evaluation

The evaporation rate, m_e can be calculated via the following equation:

$$m_e = \frac{m_h}{A} \tag{S1}$$

where, m_h is mass loss of water per hour (kg/h) due to evaporation and A is the area (m^2) of the evaporation surface.

The evaporation efficiency, η_{se} can be calculated using equation (S2).

$$\eta_{se} = \frac{m_l\,(H_{LV} + Q)}{E_{in}} \tag{S2}$$

$$H_{LV} = 1.91846 * 10^6 * [T_e/(T_e - 33.91)]^2 \tag{S3}$$

$$Q = c * (T_e - T_w) \quad \text{(S4)}$$

where, m_l = net evaporation rate (kg/m^2),

$$m_l = m_e - m_d \quad \text{(S5)}$$

m_d is the dark evaporation rate

E_{in} is the energy input of the incident light (kJ/m^{2}h),

H_{LV} is the latent heat required for vaporization of water (J/kg),

T_e is the average temperature of the solar evaporation surface,

Q is the required heat for increasing the temperature of water,

c is the specific heat of water (4.2 J/gK),

T_w is the initial temperature of the top surface of the evaporation surface.

Note S3. Salt-rejection experiment

The salt rejection property of the interfacial solar desalination evaporator holds paramount importance. The accumulation of salt can obstruct water transportation channels and impede solar absorption, ultimately leading to a reduced evaporation rate. To assess the salt-rejection capability, seawater from Whampoa Harbor, Hong Kong, was collected. Solar evaporation experiments were conducted using the CF coated with rGO and the TEG module-based solar evaporator under 1 sun illumination for a duration of 6 hours, as illustrated in Fig. S2(a). Remarkably, as depicted in Fig. S2(b) and Fig. S2(c), no salt deposits were observed on the evaporator's surface even after this extended period. Throughout the experiment, we monitored the mass loss and calculated the photothermal evaporation rate. As indicated in Fig. S2(d), the evaporation rate remained consistent at an average of 1.503 kg m^{-2} h^{-1} during the entire 6-hour duration. However, this

evaporation rate is slightly lower than the DI evaporation rate of 1.741 kg m^{-2} h^{-1}, which is owing to the higher evaporation enthalpy of seawater compared to DI water. This data conclusively validates the exceptional salt-rejection capacity of our proposed photothermal evaporator. These results underscore the reliability and effectiveness of our approach in maintaining long-term desalination performance.

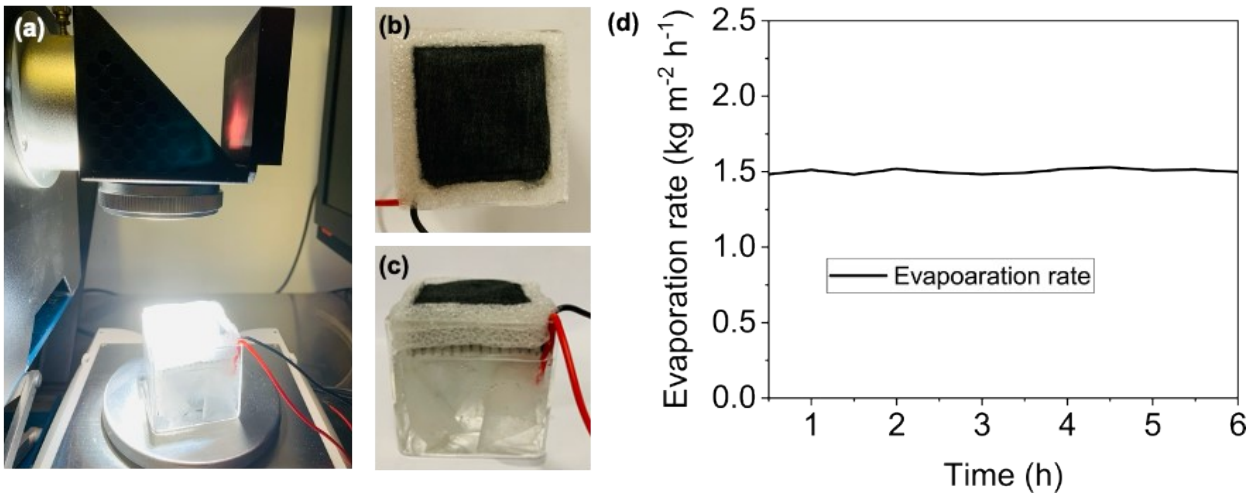

Figure S2. (a) Practical setup for salt-rejection experiment; (b) top view and (c) side view of the absorber surface after 6 hours of experiment; (d) measured water evaporation rate during the 6 h experiment.

Note S4: Water transportation ability of cotton fabric (CF)

According to the proposed design illustrated in Figure S2, the uncoated CF plays a crucial role in facilitating water transportation from the underlying bulk water to the evaporator surface. To assess the water transportation capacity of the CF, an uncoated piece of CF devoid of any rGO coating was employed. One end of the CF was submerged into a methyl red solution, while the other end was held by a tweezer. The water uptake was measured at 3 seconds and 13 seconds. The findings, illustrated in Figure S3, reveal that within a span of 10 seconds, the water uptake measures 8.1 cm, indicative of the CF's remarkable water transportation ability.

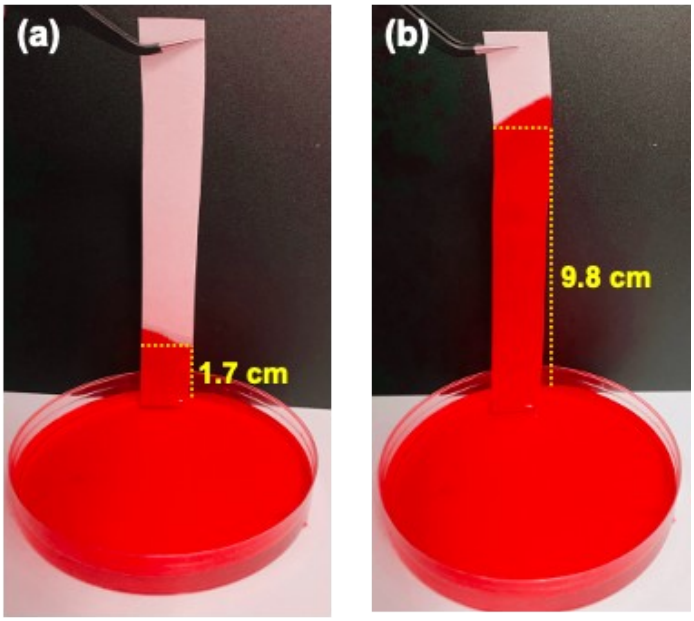

Figure S3. The water transportation ability of CF after (a) 3 sec and (b) 13 sec.

Note S5. Efficiency calculation of the TEG modules

The efficiency of the TEG modules (η), operated based on the Seebeck effect, can be written as shown in equation (S6).[1–3]

$$\eta = \left(\frac{T_H - T_C}{T_C}\right)\left[\frac{M-1}{M+\frac{T_C}{T_H}}\right] \quad \text{(S6)}$$

The conversion unit, M can be calculated from equation (S7).[1–3]

$$M = \left[1+\frac{Z}{2}(T_H + T_C)\right]^{1/2} \quad \text{(S7)}$$

The efficiency by which a material is capable of generating power, Z, can be expressed by equation (S8).[1–3]

$$Z = \left[\frac{S_H - S_C}{\sqrt{\rho_H k_H} + \sqrt{\rho_c k_c}}\right]^2 \quad \text{(S8)}$$

where,

η	=	Efficiency (%)
T_H	=	Hot side temperature of the TEG (K)
T_C	=	Cold side temperature of the TEG (K)
M	=	Conversion Unit
Z	=	Efficiency with which a material can generate power (K^{-1})
S_H	=	Seebeck coefficient for hot material (For n-type Bismuth Telluride the value is -228 μV/K)
S_C	=	Seebeck coefficient for cold material (For p-type Antimony Telluride the value is 185 μV/K)
ρ_H	=	Electrical conductivity of hot material (For n-type Bismuth Telluride the value is 12.6 μΩm)
ρ_c	=	Electrical conductivity of cold material (For p-type Antimony Telluride the value is 12.6 μΩm)
k_H	=	Thermal conductivity of hot material (For n-type Bismuth Telluride the value is 1.8 W/mK)
k_C	=	Thermal conductivity of cold material (For p-type Antimony Telluride the value is 1.3 W/mK)

From the experimental value, the hot side and cold side temperatures of the TEG module are found to be:

T_H = 37.2 °C = (37.2 + 273.15) K = 310.35 K

T_C = 16.2 °C = (16.2 +273.15) K = 289.35 K

Therefore, from equations (S8) and (S7) the value of Z and M can be calculated respectively.

$$Z = \left[\frac{-228-185}{\sqrt{12.6\times 1.8}+\sqrt{12.6\times 1.3}}\right]^2 = 2197.811\ K^{-1}$$

$$M = \left[1+\frac{2197.811}{2}(310.35+289.35)\right]^{1/2} = 811.7971$$

Finally, the efficiency can be calculated from equation (S6).

$$\eta = \left(\frac{T_H - T_C}{T_C}\right)\left[\frac{M-1}{M+\frac{T_C}{T_H}}\right] = \left(\frac{310.35-289.35}{289.35}\right)\left[\frac{811.7971-1}{811.7971+\frac{289.35}{310.35}}\right]$$

$$\eta = 0.073\times 0.998 = 0.073\times 100\% = 7.3\%$$

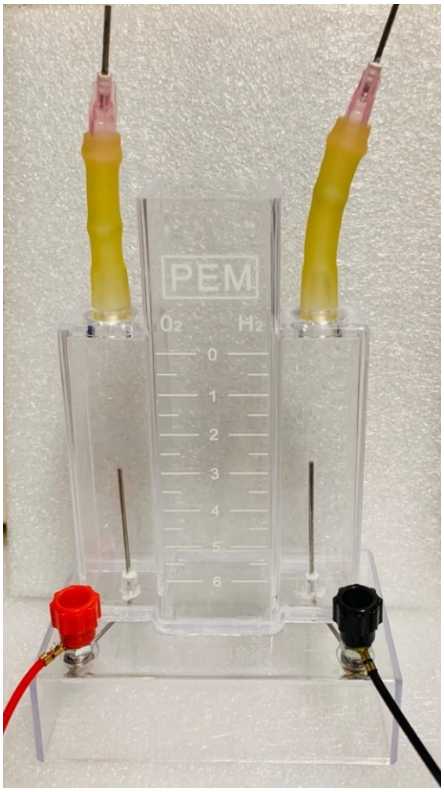

Figure S4. Custom-made Hoffman apparatus for conducting the hydrogen production experiments.

Note S6. Thevenin Equivalent resistance and duty cycle calculation for transferring maximum power

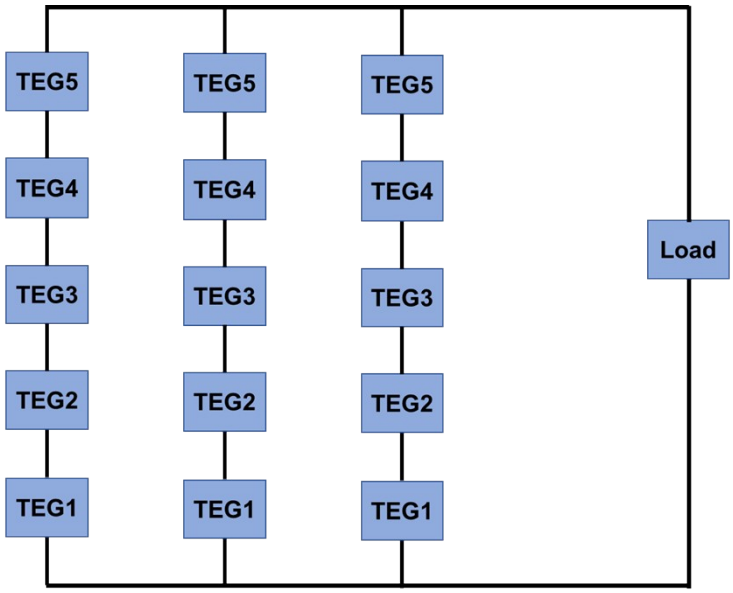

Figure S5. Series parallel combination of the TEG modules

The internal resistance of each TEG module was measured as 6.1Ω. Therefore, the Thevenin equivalent resistance can be calculated as 10.17 Ω.

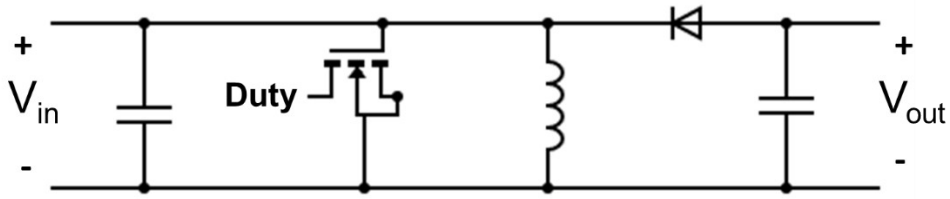

Figure S6. Buck-boost converter circuit

The input-output equation of the buck-boost converter can be expressed by equation (S9).

$$V_0 = \left(\frac{D}{1-D}\right)V_{in} \tag{S9}$$

Neglecting the switching loss, the input and output power can be considered the same for the DC-DC converter circuit.

$$P_0 = P_{in}$$

$$\frac{V_0^2}{R_0} = \frac{V_{in}^2}{R_{in}} \quad => \frac{\left(\frac{D\,V_{in}}{1-D}\right)^2}{R_0} = \frac{V_{in}^2}{R_{in}} \quad => \left(\frac{D}{1-D}\right)^2 = \frac{R_0}{R_{in}}$$

$$\frac{D}{1-D} = \sqrt{\frac{R_0}{R_{in}}} \quad => \frac{D+1-D}{D-1+D} = \frac{\sqrt{R_0}+\sqrt{R_{in}}}{\sqrt{R_0}-\sqrt{R_{in}}}$$

$$\frac{1}{2D-1} = \frac{\sqrt{R_0}+\sqrt{R_{in}}}{\sqrt{R_0}-\sqrt{R_{in}}} \quad => 2D-1 = \frac{\sqrt{R_0}-\sqrt{R_{in}}}{\sqrt{R_0}+\sqrt{R_{in}}}$$

$$D = \frac{\sqrt{R_0}}{\sqrt{R_0}+\sqrt{R_{in}}}$$

$R_0 = R_L = 190.12\Omega$ and $R_{in} = R_{opt} = 10.17\ \Omega$

$$D = \frac{1}{1+\sqrt{\frac{R_{opt}}{R_L}}} \tag{S10}$$

Putting the values into these equations, the value of duty cycle (D) becomes 81%.

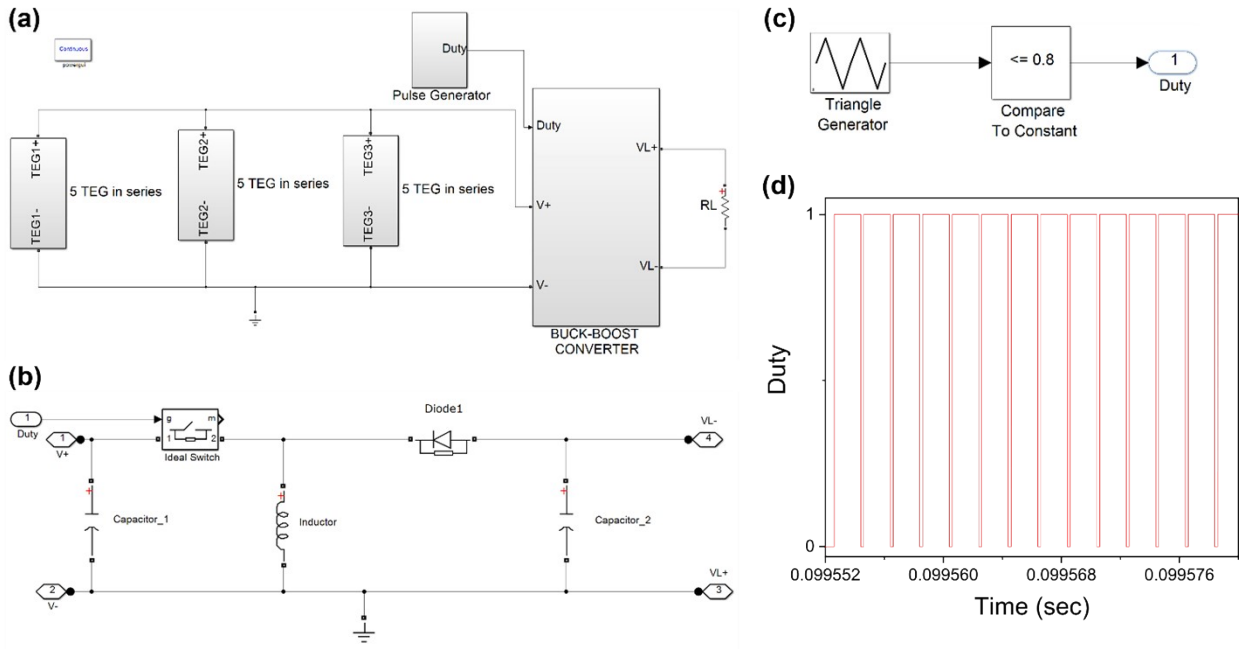

Figure S7. (a) A schematic diagram of the simulated circuit; (b) the buck-boost converter circuit; (c) the simulated circuit for 81% duty generation; (d) the waveform of the generated duty cycle.

Note S7. Hydrogen and oxygen generation reactions

At 25 °C and 1 atm pressure, the water electrolysis equations for hydrogen and oxygen generation from alkaline medium can be written as follows:

Cathode $2H_20 + 2e = H_2 + 2OH^-$ $E_c^0 = -0.83\ V$

Anode $2OH^- = H_2O + {}^1/_2O_2 + 2e$ $E_a^0 = 0.40\ V$

with the total reaction expressed as follows:

$H_2O = H_2 + {}^1/_2O_2$ $U^0 = 1.23\ V$

U^0 is known as theoretical decomposition voltage, which is a thermodynamic parameter, and has the value 1.23 V at 25 °C and 1 atm pressure.

Note S8. Performance comparison

Table S1. Solar steam generation performance comparison

Evaporation material	Evaporation rate under 1 sun [kg m^{-2} h^{-1}]	Maximum Evaporation Efficiency	Ref.
Carbonized daikon	1.57	85.9%	[4]
Biomass based carbon particles (CPs)			
$coffee_{-600-0.03}$	1.49	76%	[5]
$rose_{-600-0.03}$	1.65	93.4%	
$straw_{-600-0.03}$	1.69	92.8%	
Carbonized lotus seedpod	1.30	86.5%	[6]
SM-LS	1.30	79.98%	[7]
Ag nanoparticles coated on bamboo	0.96	~87%	[8]
TiN nanoparticles on carbonized wood	1.26	92.5%	[9]
Deep eutectic solvents decorated wood	1.3	89%	[10]
Fe^{3+} ion loaded wood	1.85	~90%	[11]
$CuFeSe_2$ nanoparticle coated wood	~1.3	~70%	[12]
WO_{3-x} nanorod decorated wood	~6.1	~82.5%	[13]
MoS_{2-x} NSAs	1.32	80.3%	[14]
rGO coated cotton fabric	1.385	86.98	This work

References:

[1] K. Ono, R. O. Suzuki, *JOM* **1998**, *50*, 49.

[2] D. M. Rowe, *Renew Energy* **1999**, *16*, 1251.

[3] H. Takazawa, H. Obara, Y. Okada, K. Kobayashi, T. Onishi, T. Kajikawa, in *2006 25th International Conference on Thermoelectrics*, IEEE, **2006**, pp. 189–192.

[4] M. Zhu, J. Yu, C. Ma, C. Zhang, D. Wu, H. Zhu, *Solar Energy Materials and Solar Cells* **2019**, *191*, 83.

[5] H. Jiang, X. Geng, S. Li, H. Tu, J. Wang, L. Bao, P. Yang, Y. Wan, *J Mater Sci Technol* **2020**, *59*, 180.

[6] J. Fang, J. Liu, J. Gu, Q. Liu, W. Zhang, H. Su, D. Zhang, *Chemistry of Materials* **2018**, *30*, 6217.

[7] A. M. Saleque, S. Ma, S. Ahmed, M. I. Hossain, W. Qarony, Y. H. Tsang, *Adv Sustain Syst* **2021**, *5*, 2000291.

[8] C. Sheng, N. Yang, Y. Yan, X. Shen, C. Jin, Z. Wang, Q. Sun, *Appl Therm Eng* **2020**, *167*, 114712.

[9] D. Guo, X. Yang, *Sci China Mater* **2019**, *62*, 711.

[10] Z. Chen, B. Dang, X. Luo, W. Li, J. Li, H. Yu, S. Liu, S. Li, *ACS Appl Mater Interfaces* **2019**, *11*, 26032.

[11] F. He, M. Han, J. Zhang, Z. Wang, X. Wu, Y. Zhou, L. Jiang, S. Peng, Y. Li, *Nano Energy* **2020**, *71*, 104650.

[12] H. Liu, C. Chen, H. Wen, R. Guo, N. A. Williams, B. Wang, F. Chen, L. Hu, *J Mater Chem A Mater* **2018**, *6*, 18839.

[13] Z. Li, M. Zheng, N. Wei, Y. Lin, W. Chu, R. Xu, H. Wang, J. Tian, H. Cui, *Solar Energy Materials and Solar Cells* **2020**, *205*, 110254.

[14] B. Yuan, L. Yang, H. Yang, L. Bai, W. Wang, D. Wei, Y. Liang, H. Chen, *Energy Convers Manag* **2022**, *252*, 115070.